A CONTINENTAL SCALE MOSAIC OF THE AMAZON BASIN USING JERS-1 SAR

P. Siqueira[1], S. Hensley[1], S. Shaffer[1], L. Hess[2],
G. McGarragh[1], B. Chapman[1], and A. Freeman[1]
[1]Jet Propulsion Laboratory, California Institute of Technology
4800 Oak Grove Drive, Pasadena, CA 91109, USA
[2]Institue for Computational Earth System Science, University of California,
Santa Barbara, CA 93106, USA

ABSTRACT

In this paper, a methodology, example, and accuracy assessment are given for a continental scale mosaic of the Amazon River basin at 100 m resolution using the JERS-1 satellite. This unprecedented resource of L-band SAR data collected by JERS-1 during the low-flood season of the river, amounts to a collection of 57 orbits of the satellite and a total of some 1500 1k x 1k byte images. Interscene overlap both in the along-track and cross-track directions allows common reference points to be used to correct for individual scene geolocation inaccuracies which have been derived from the satellite ephemeris. The set of common reference points is assembled into a matrix formulation which is used to solve for individual scene geometric offsets. By correcting for these offsets, each scene is placed within a global coordinate system which can then be used as the basis for creating a final, visually seamless mosaic. The methodology employed in this approach allows for a mathematical foundation to be applied to the mosaicking process as well as providing a unique, traceable solution for correctly geolocating satellite imagery.

I. INTRODUCTION

The purpose of this paper is to describe and demonstrate a methodology for the mosaicking of continental-scale SAR data sets. The particular example that will be used is the single-season (September-December 1995) 1500-scene JERS-1 data set collected for the Global Rain-Forest Mapping (GRFM) project [Rosenquist, 1996] initiated by the National Space Development Agency of Japan (NASDA). Proper mosaicking of scenes while minimizing distortion is critical for performing large-scale regional analysis and for data fusion (Figure 1). The method presented in this paper utilizes a matrix inversion to position individual scenes correctly with respect to one another. This simultaneous solution allows for the position errors to be minimized over a global context as well as providing a degree of mathematical traceability. It will be shown that the result of this treatment corrects the positioning errors for each scene to within 400 meters and yields information about the source of those inaccuracies.

The general philosophy for constructing the Amazon mosaic is to separate the functions of mosaicking and geolocation. Although the step of mosaicking can take on a number of variations, the process is fairly straight forward and will not be the primary subject of this paper. More importantly, and preceding the step of mosaicking is that of geolocation, or determining with some degree of accuracy the proper location of scenes within a global context. The physical location of a scene on a global scale may be initially estimated by knowledge of the satellite path, time of day, etc. using the satellite ephemeris [Curlander, 1982]. Geolocation accuracy of this sort for JERS-1 is typically on the order of 5 km [Chapman et al., 1998]. Ideally, we would like to have the geolocation known to the full resolution of the instrument. Once individual scenes are properly geolocated, the process of mosaicking becomes a simple image processing task of how to combine and resample the data into a standard output format.

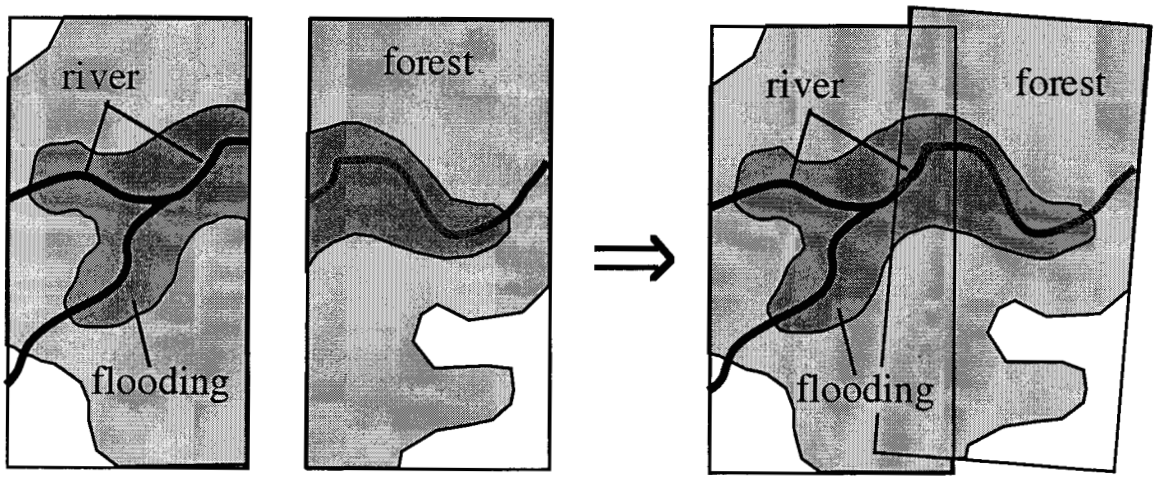

Figure 1 *Example of two individual scenes before and after geolocation and mosaicking. Proper mosaicking of the images allows for accurate estimates to be made of extended features such as river lengths, flooded areas and deforested regions.*

The method described here makes substantial use of the overlap region between adjacent images. Overlap between scenes allows for relative positioning of images with respect to one another. Although there are a number of methods for combining data from different scenes, the method commonly employed [Kwok, Curlander and Pang, 1990] follows a straightforward set of steps. These are,

1. one scene is fixed in space (i.e. the estimated location of the scene is assumed correct).
2. the second scene is placed relative to the first scene, using its own satellite estimated geolocation.
3. small pieces of the common areas between the two images are extracted and cross-correlated to determine the relative shift between the two images. The shifts estimated in this step may be different for each small piece (Figure 2).
4. Pixel locations of the new scene are transformed (preferably by a linear transformation) to correct for the shifts calculated in the previous step.
5. The data from the two scenes are combined to make up a single, larger scene.

6. The combined scene becomes the reference scene and we return to step 1 to introduce additional data as desired.

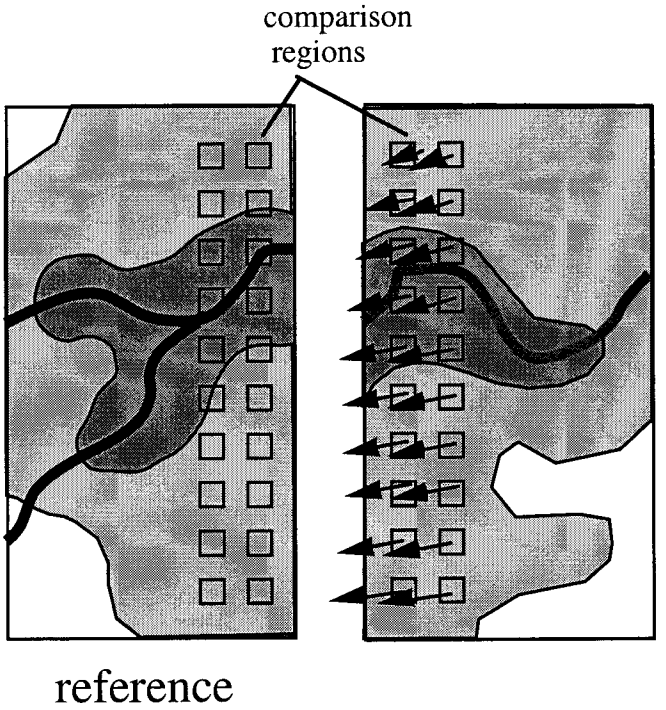

Figure 2 *Illustration of the "matching" between a reference scene and an adjacent scene. Shifts for each small area are calculated to maximize the autocorrelation. These shifts may later be used for determining a total shift and rotation for the floating scene.*

Generally speaking, the above outline for the process of mosaicking is the course typically taken when performing the procedure by hand. When working with a small number of scenes, it is an efficient approach. Problems arise however if a large number of scenes are required to be mosaicked together as in the Amazon mosaic, which covers the northern component of the South American continent (approximately 8 million km^2 or 35,000 x 41,000 100 meter pixels; these numbers are not precisely equivalent because the imaged area is not equivalent to the rectangular shape of the mosaicked image). This is because small errors or misalignments made with adjacent scenes relative to the reference scene will propagate and become larger the farther away scenes are from the reference location. This method of mosaicking is akin to wallpapering, where one strip of paper is fixed in space, while other strips are

propagated outward. As the distance from the reference scene (i.e. the first piece of wallpaper) increases, new scenes may not fit together very well (Figure 3). Placement of new scenes will rely on a balance of the errors between the new scene and the scenes already fixed in space. In addition to not having a uniformly distributed error allocation, the mosaic derived by the wallpaper method is non-unique, dependent upon the order that new scenes are added to the mosaic. What is desirable is to develop is a single, unified approach for correcting interscene geolocations.

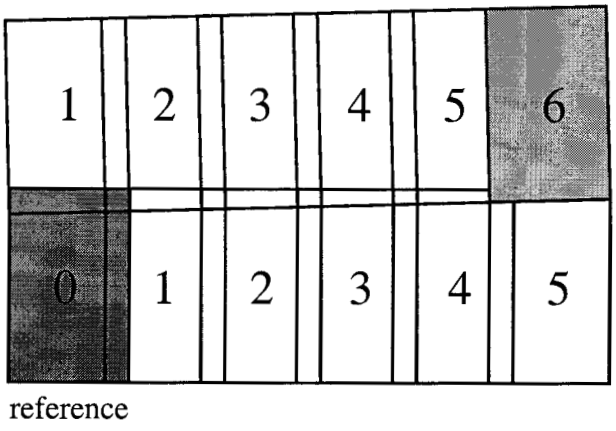

Figure 3 *Illustration of how errors propagate when the wallpaper method of mosaicking is used. Numbers within the individual scenes indicate the ordering in which the scenes were mosaicked (i.e. the mosaic itself is non-unique). Errors increase with the distance from the reference scene.*

The solution to this problem is to allow the images to float with respect to one another until the locations of all scenes are calculated simultaneously. Steps 1 through 3 from the general method still remain the same, but the final calculation of the transformation is left until all of the scenes in the mosaic have gone through the initial steps. The complete matrix solution incorporates all of the information that has been assembled, thus allowing the geolocation errors to be minimized in a global context rather than a local one.

II. FORMULATION

The process described in this paper, specific for the continental mosaic of the Amazon region, or any large-scale image, is a reduced version of a three-dimensional set of routines written by Hensley and Shaffer [work in progress] used for combining three-dimensional interferometric SAR data sets. Here, the problem is simplified to work in two dimensions, but the scale of the final mosaic is intended to cover a very extended area.

The production of the final mosaic is the result of a four-step process

1. Determination of match points
2. Removal of 'noisy' data (referring to bad match points)
3. Simultaneous solution of geometric correction factors
4. Generation of mosaicked image.

The process can best be described by the example of geolocation of two image scenes.

A. Two-Scene Problem

We begin by describing the intensity, $I_i(\bar{x})$, of image, i, as being a function of position, $\bar{x}$, relative to a global coordinate system. Allowing for a linear set of transformations to be applied to the entire image, any point within that image may be transformed as

$$\bar{x}' = \overline{\overline{M_i}}\bar{x} + \overline{T_i} \quad . \qquad (2)$$

where $\overline{\overline{M_i}}$ is a matrix relating to geometric distortion composed of rotation, skew and scaling terms, and $\overline{T_i}$ is a two-dimensional translation vector. Our goal is first to determine the relative shifts for a variety of points between two images and then to translate those shifts into a linear transform that may be described by (2). The shift, $\overline{x_n}$,for the n^{th} point in the image can be found relative to a reference image using a simple pattern matching procedure, such as the cross-correlation. The shift, $\overline{\varepsilon_{ij}}(\overline{x_n})$, is defined as the location of the maximum value of the cross-correlation, as in

$$\overline{\varepsilon_{ij}}(\overline{x_n}) = \overline{m_{max}\Delta x} \tag{3}$$

which is defined as

$$\overline{m_{max}\Delta x} = \max_{m} \left[\frac{1}{K} \sum_{k\Delta x}^{neigh} I_i(\overline{x_n} + \overline{k\Delta x}) \cdot I_j(\overline{x_n} + \overline{k\Delta x} + \overline{m\Delta x}) \right] \tag{4}$$

for all m. In (4), Δx is the sample spacing, which may be different between latitude and longitude, and K is the total number of pixels used in the summation local to the neighborhood (*neigh*) of $\overline{x_n}$ and $\overline{m\Delta x}$ effectively shifts one image relative to the other until the correlation achieves a maximum. Each observation of $\overline{\varepsilon_{ij}}(\overline{x_n})$ can be modeled as

$$\overline{\varepsilon_{ij}}(\overline{x_n}) = \left\{ \overline{\overline{M_i}} \left[\overline{\overline{A_i}}\,\overline{x_n} + \overline{B_i} \right] + \overline{T_i} \right\} - \left\{ \overline{\overline{M_j}} \left[\overline{\overline{A_j}}\,\overline{x_n} + \overline{B_j} \right] + \overline{T_j} \right\} \tag{5}$$

where $\overline{\overline{A_i}}, \overline{B_i}, \overline{\overline{A_j}}, \overline{B_j}$ are the linear transforms inducing the geolocation errors that we would like to determine. While individual components of the matrices can be estimated, ideally we would like to relate those components to actual image transformations, so that those transformations can be constrained according to the distortion model being employed. Thus, the matrices, $\overline{\overline{A}}$ and $\overline{\overline{M}}$ can be written as a combination of a rotation,

$$\overline{\overline{R}} = \begin{bmatrix} \cos\theta & \sin\theta \\ -\sin\theta & \cos\theta \end{bmatrix} \tag{6}$$

skew,

$$\overline{\overline{Q}} = \begin{bmatrix} 1 & 0 \\ q & 1 \end{bmatrix} \tag{7}$$

and scale,

$$\overline{\overline{\Lambda}} = \begin{bmatrix} \lambda_x & 0 \\ 0 & \lambda_y \end{bmatrix} \tag{8}$$

such that

$$\overline{\overline{A}} = \overline{\overline{R}}\,\overline{\overline{Q}}\,\overline{\overline{\Lambda}}. \tag{9}$$

The vectors $\overline{B}$ and $\overline{T}$ represent coordinate translations, as in

$$\overline{B} = \begin{bmatrix} t_x \\ t_y \end{bmatrix}. \tag{10}$$

Thus, the functional form of the observation vector can be rewritten as a function of position and the unknown parameters, $\overline{\varepsilon_{ij}}(\overline{x_n};\overline{Z})$, where $\overline{Z}=\{\theta,q,\lambda_x,\lambda_y,t_x,t_y\}$. Solution of (5) for the components of $\overline{Z}$ is a nonlinear problem. Assuming small values for $\overline{Z}$ however, we can linearize (5) by taking derivatives with respect to the unknowns

$$\overline{\varepsilon_{ij}} \approx \sum_{\zeta\in\overline{Z}} \frac{\partial\varepsilon}{\partial\zeta}\Delta\zeta = \overline{\overline{J}}\,\overline{Z} \tag{11}$$

where $\overline{\overline{J}}$ is the Jacobian. For the two-scene problem above, the dimension of $\overline{\overline{J}}$ is $2xN$, where N is the number of parameters in $\overline{Z}$ that we are solving for. Each row in (11) represents the component of $\overline{\varepsilon_{ij}}$ along one of the vector dimensions, $\hat{x}$ or $\hat{y}$. For a total of P observations, the dimension of $\overline{\varepsilon_{ij}}$ is $2Px1$ and $\overline{\overline{J}}$ is $2PxN$.

To solve for $\overline{Z}$ in (11), the number of observations must be greater than the number of unknowns and should be well distributed across the common area between the two images being mosaicked. To preserve memory and to increase the efficiency of inverting (11), like rows of $\overline{\varepsilon_{ij}}$ and $\overline{\overline{J}}$ (i.e. $\overline{\varepsilon_{ij}}\cdot\hat{x}$ and $\overline{\varepsilon_{ij}}\cdot\hat{y}$) may be summed to reduce their dimensions to $2x1$ and $2xN$ respectively. Using a least squares approach the vector of unknowns can be found by

$$\overline{Z}=\left(\overline{\overline{J}}^t\,\overline{\overline{J}}\right)^{-1}\overline{\overline{J}}^t\,\overline{\varepsilon_{ij}}, \tag{12}$$

where the superscript, t, refers to a matrix transpose. The term

$$\overline{\overline{U}}=\overline{\overline{J}}^t\,\overline{\overline{J}} \tag{13}$$

is a positive semi-definite matrix whose components consist of the double derivative of the observation with respect to the unknowns.

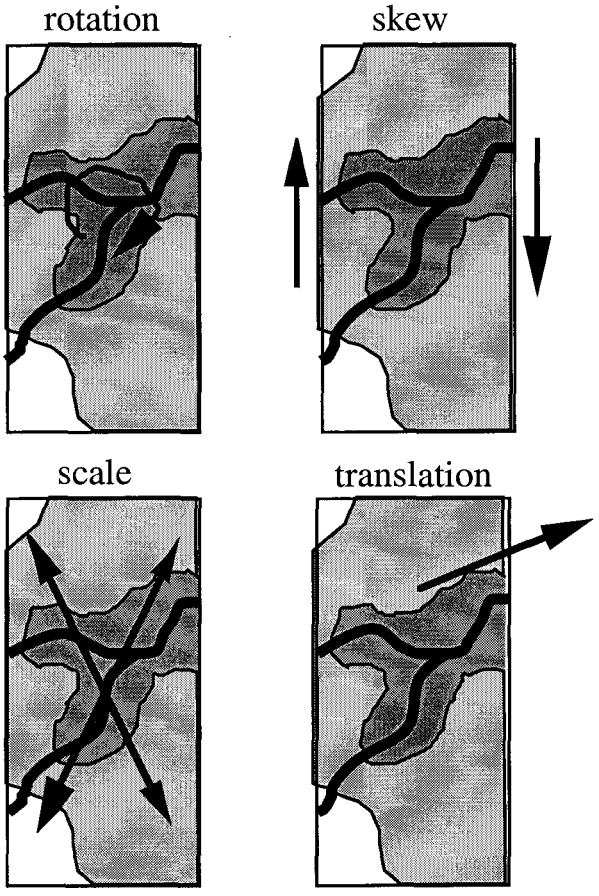

Figure 4 *Illustration of the four linear transformations allowed for each image (scale, translation, rotation and skew).*

B. N-Scene, continental mosaic

Solution of (12) requires a simple matrix inversion. For a two-scene problem, there can be no more than six unknowns to solve for; for N scenes, we have 6(N-1) unknowns since one scene must remain fixed as a reference. For the 1500-scene JERS-1 Amazon coverage, this could amount to 9000 unknowns, a large matrix inversion task. The advantage to this methodology however is that the structure of $\overline{\overline{U}}$ is such that it directly reflects the geometrical organization of the satellite data. That is, for a slowly precessing orbit and uniform scene size, any one scene will have no more than eight neighbors, designated N_{neigh}. Similarly, in the matrix expansion of (12), there will be a maximum of $6N_{\text{neigh}}$ elements contributing to any given row of the matrix.

Thus $\overline{\overline{U}}$ will have the desirable properties of being both sparse and banded as well as symmetric (Figure 5). Thus, a sparse matrix solver like DPBSV of LAPACK [Anderson et al., 1990] can be employed to solve for $\overline{Z}$ and considerably increase computational efficiency.

In this example for the Amazon mosaic, it was assumed that the processor delivered individual scenes that were geometrically accurate, i.e. scaling and skewing distortions were not present in the output product. Thus, the number of unknowns that the geolocation algorithm needed to solve for was three: two for translation in latitude and longitude, and one for rotation about the radial axis. Numerically, the reduction in unknowns has the effect of speeding up the matrix inversion, as well as delivering a more stable solution set (i.e. the matrix will be less likely to have singular values).

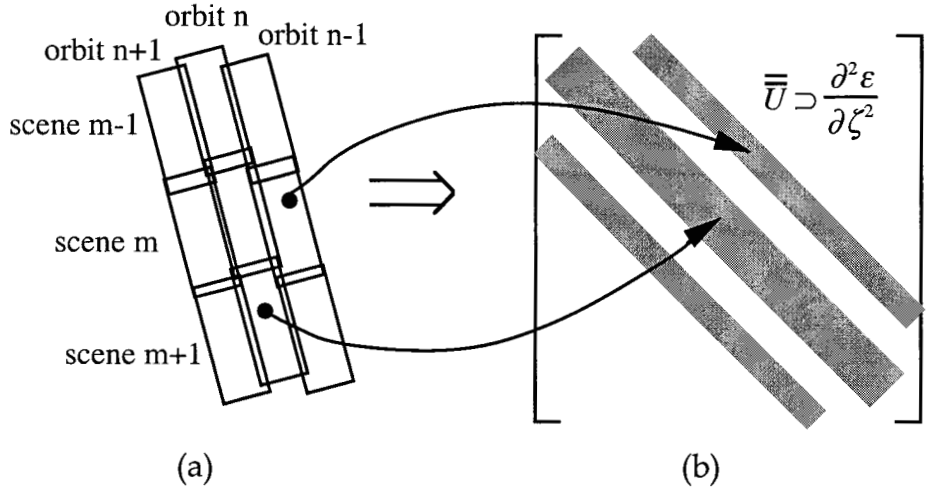

Figure 5 *Relationship between the orbital geometry (a) and the shaded non-zero elements of the* $\overline{\overline{U}}$ *matrix (b). In the example, the orbital geometry is arranged by scene number first, then orbit number.*

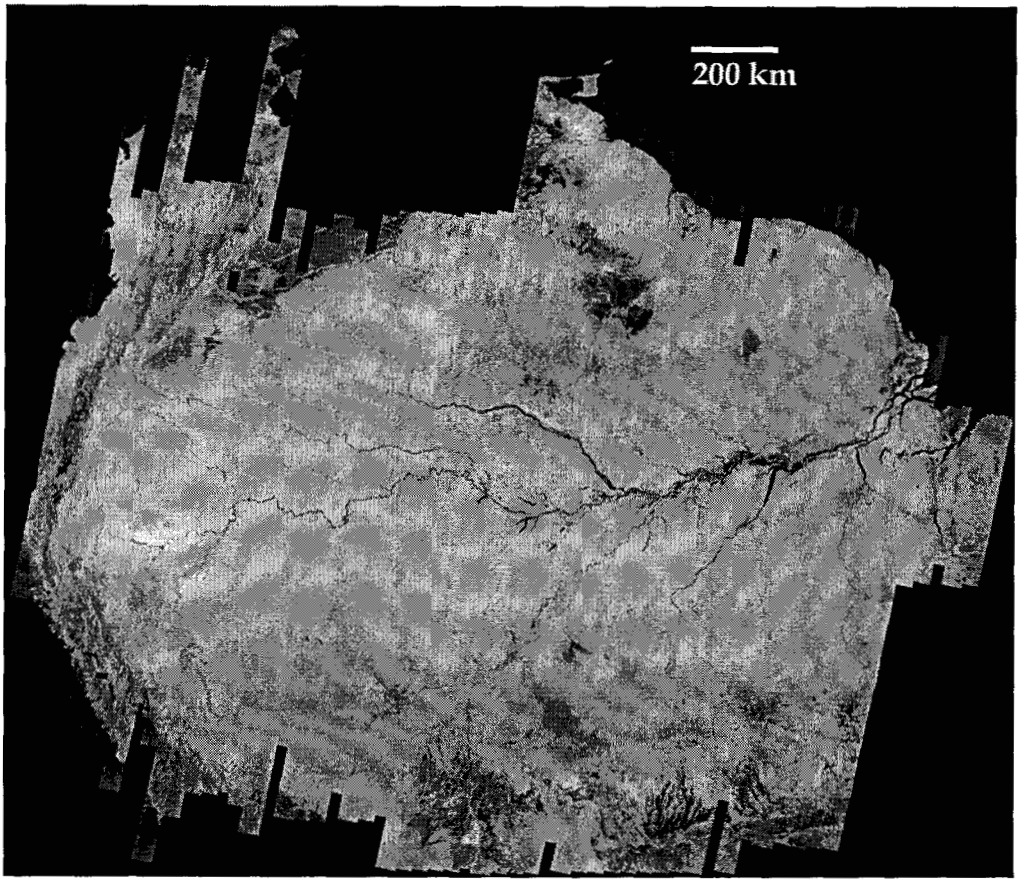

Figure 6 *Complete 1500-scene mosaic of the Amazon basin and surrounding area. The mosaic is bounded in the west by the Andes and the Pacific Ocean, to the east by the mouth of the Amazon River, to the North by Guyana (data over Venezuela was not collected) and to the South by the 14 degree longitude line. In all, most of the mosaic comprises some 8 million square kilometers. The dimension of the image above is 35,000 pixels in latitude and 41,000 pixels in longitude with an equiangular pixel spacing of 3 arcseconds.*

III. Geometric and Ephemeral Data Accuracy

To check the geometric accuracy of the final mosaic, 57 control points were located on 1:50,000 to 1:100,000 scale maps of Brazil, Peru, Bolivia, Columbia, Ecuador and Trinidad. Features commonly used in locating control points on optical imagery, such as road intersections and airstrips, could not be distinguished from roadside open areas; roads in forested areas were often obscured by trees. Confluence of streams with channel widths of 100 to 300 m provided the most reliable control points. Care was taken to avoid locating points where floodplain geomorphology indicated active channel migration, or

where apparent control point location was likely to vary between high- and low-flood stages. All points were located on flat or moderate terrain, since currently available digital elevation models are not sufficiently accurate to perform terrain corrections on the mosaic.

Map locations were determined manually using a ruler; accuracy of map coordinate locations was judged to range from 0.5-2.0 mm of map distance. . Control point locations were transformed from map datums to the WGS 84 datum. Ninety-five percent of the points on the map sheets were estimated to be locatable to within 1 mm or less, corresponding to a ground uncertainty of 100 m, the approximate pixel size of the mosaic. All points within the radar mosaic were judged to be locatable to within two pixels, 60% of which were locatable within one pixel

The location of the control points and the vector differences between the mosaic and the ground control points are shown in Figure 7, where the magnitudes of the errors have been exaggerated by a factor of 100 for clarity. The errors shown in this plot indicate that a large scale rotation and shift is present in the data. This is an unsurprising result since in its primary form, the geolocation of the individual scenes of the mosaic was only self-consistent, using a single scene for a reference, and did not include any data that physically correlated with known locations on the ground.

The similarity in size and angle of the difference vectors for geographically proximate points (Figure 7) indicates the high accuracy of locating control points, and the geometric consistency of the mosaic within small regions. The accuracy over small regions was evaluated by separating the points into clusters of points within one degree latitude and longitude of each other, and applying an average geolocation correction to each cluster. The mean geolocation error for all points, comparing them with points within their clusters, was 38 m in latitude and 32 m in longitude.

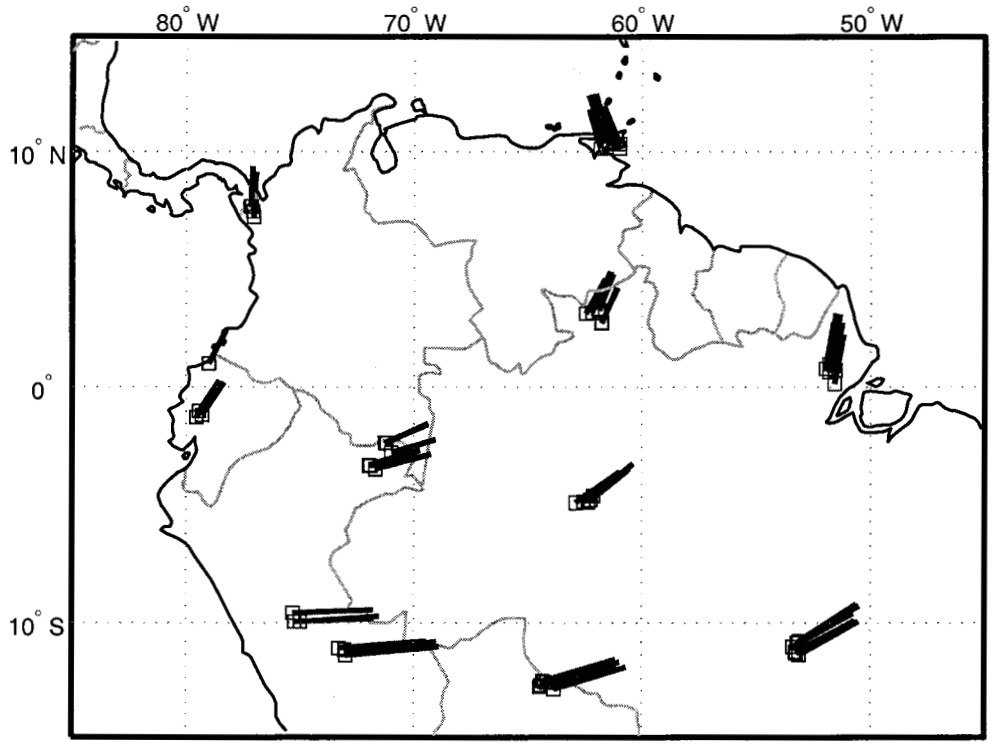

Figure 7 *Geolocation errors for the Amazon mosaic. Evident in the pattern of the errors is a large-scale rotation and shift of the mosaic with respect to the geography. The magnitude of error vectors has been scaled by a factor of 100 for illustration. Boxes indicate map locations.*

Inclusion of ground control points into the inversion matrix for determining the location of individual scenes of the mosaic is the equivalent of adding a single, pan-continental scene that is not allowed to undergo any transformation (i.e. it is regarded as the 'truth-scene'). The known locations of landmarks within the ground control point scene are manually matched to features within individual scenes, which serve as the observation vector for the truth-scene. This alters the geometry of the $\overline{\overline{U}}$ matrix in that it adds an extended vertical and horizontal row since the one scene has common elements with a large number of other scenes within the mosaic. This has the effect of disturbing the computational advantage of the matrix banding, but still, significant computational advantage can be gained by exploiting the symmetrical, positive semi-definite characteristic of the matrix.

For the Amazon mosaic, from the total of 57 ground control points that were available for use, 27 were used to tie down the mosaic, and the remaining 30 were used to estimate the geolocation accuracy. The points were chosen by first breaking them into twelve geographically distinct groups. From the twelve groups, six were chosen to fix the mosaic and six were chosen as test groups. The tie-point groups were chosen such that they would span the topographically flat region of the Amazon basin. A flat region was chosen so as not to incur potential scaling problems for the region to the west of the continent covered by the Andes, where the processor typically does not take into account the change in topography.

Once the tie points were chosen and incorporated as a truth-scene into the matrix inversion, the remaining points were tested to estimate the residual geometric distortion. A graphic summary of the results is shown in Figures 8 and 9. Figure 8 illustrates the location of the ground control and test points within the mosaic, as well as the direction of the errors. In Figure 9, we show histograms of the geolocation errors at three points in the geolocation process. The first histogram summarizes the shifts required between individual scenes so that they make a visually continuous mosaic. These errors are ultimately related to the satellite ephemeris (to be discussed shortly). The second and third histograms of Figure 9 show the magnitude of geolocation errors for the situations where tie points were not or were used to fix the mosaic to a global reference. The magnitude distribution of the geolocation errors for the mosaic using tie points is 0.0 ± 400m. As a result of this analysis, we can make the following observations:

1. There does not seem to be any effect of topography on the geolocation accuracy. That is, the westernmost points across the Andes mountain ranges had geolocation accuracies on the order of 100 meters.

2. Geolocation errors are longitudinally directed are proportional in sign and magnitude to latitude. The source of this effect is unknown as of this writing.
3. Average geolocation error across the mosaic is 400m, which is roughly 0.01% of the entire width of the mosaic.

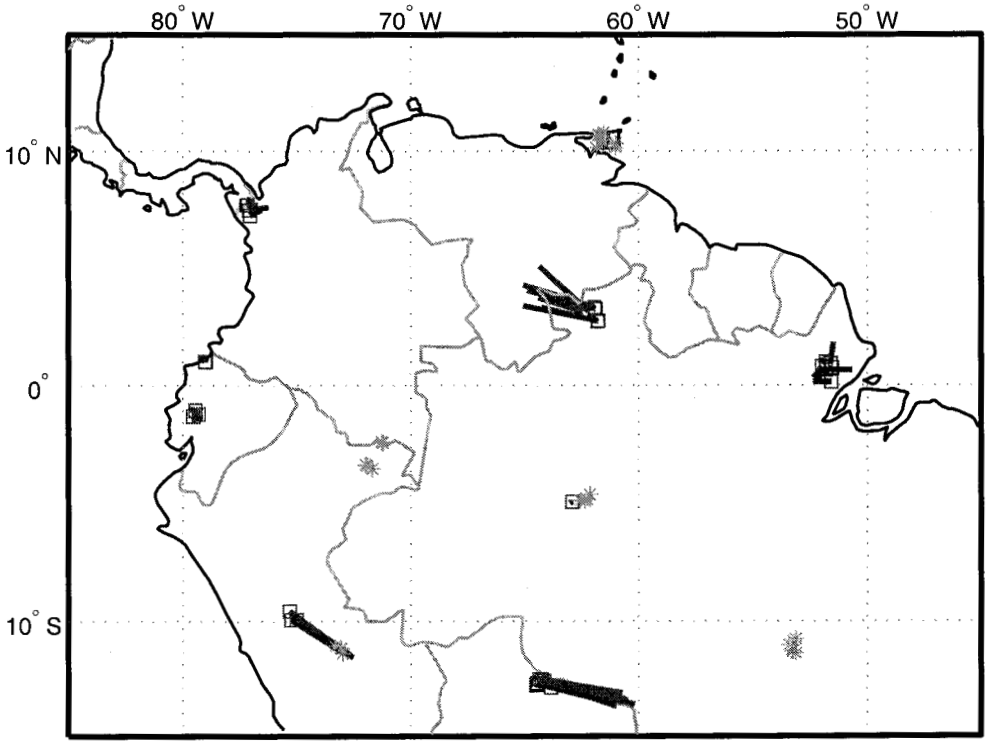

Figure 8. *Location of ground control points (i.e. tie points) shown as asterisks, and test points, shown as squares with vector lines indicating the direction and magnitude (scaled by a factor of 600) of geolocation errors. The mean error is on the order of 400 meters, or four pixels out of 35,000.*

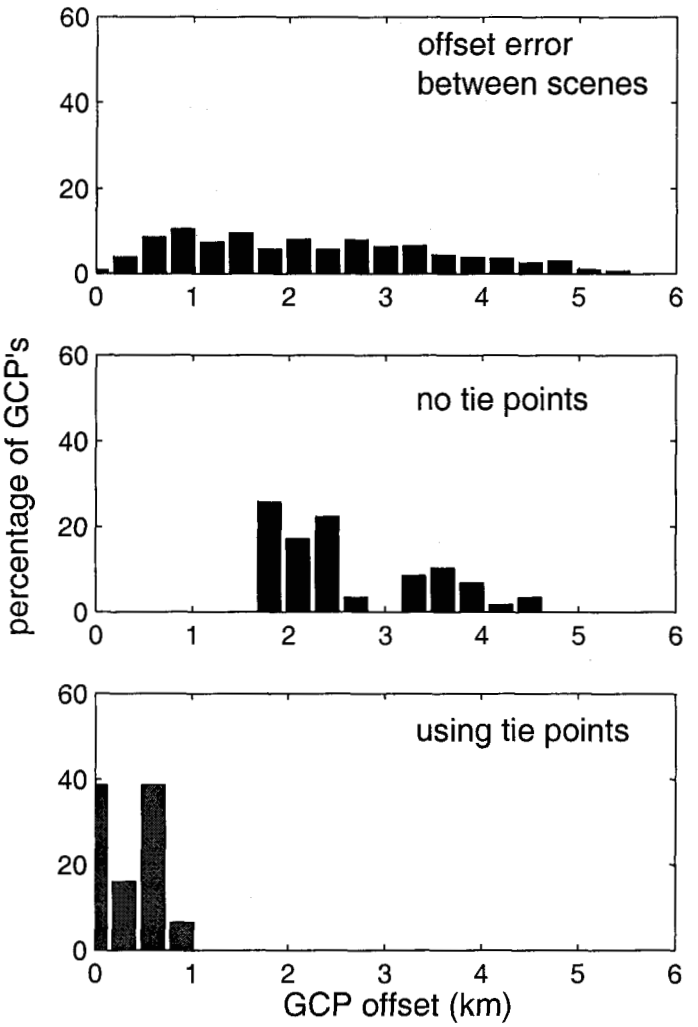

Figure 9 *Histogram of geolocation errors for the three mosaics discussed in this article: i) mosaic using satellite ephemeris only, ii) self-consistent accounting for scene rotation and shifts but using no ground control points, and iii) mosaic accounting for scene rotation and shifts and using 27 ground control points distributed in six groups across the Amazon basin.*

Because the overall geolocation accuracy is so accurate, it is possible to look at the translation offsets of the individual scenes to gain some insight into the source of the errors in the satellite ephemeris, which is used to determine the location of individual scenes within a global coordinate system [Curlander, 1982]. Figure 10 shows the offset adjustments calculated for each scene using the geolocation algorithm as a function of the scene position on the continental mosaic. In this figure the largest offsets can be seen to be dominated by a cross track component that oscillates on the order of every ten orbits of the satellite.

This is most likely due to an update of the internal satellite clock [Shu-mada, JPL/NASDA personal communication, 1997] which had not been taken to account in the Alaska SAR facilities processing of the JERS-1 data (but is incidentally, accounted for in the NASDA processor).

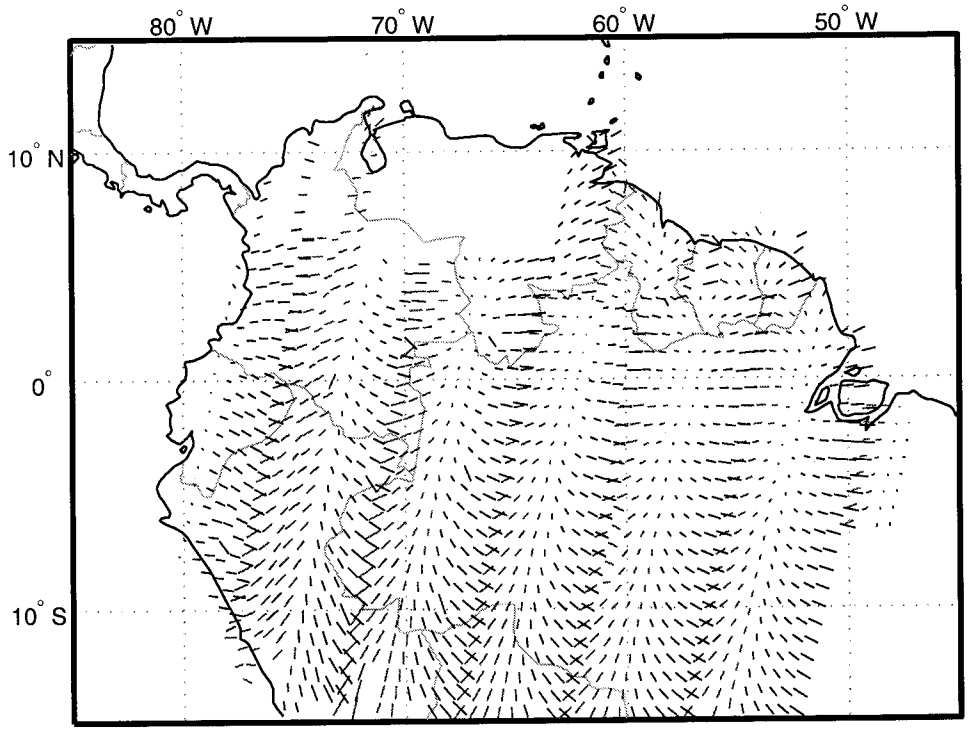

Figure 10. *Individual scene offsets determined by the geolocation algorithm discussed in this paper. The direction of the errors sweeps from right to left and then resets every ten orbits as a result of a timing correction to the satellite's internal clock.*

V. Conclusion

In this paper we have presented a method for assembling continental-scale data sets into a single mosaic. The numerical technique employed allows for a simultaneous solution for determining the correction factors for individual scenes. This has the effect of balancing out individual errors across the entire region (rather than fixing them and causing them to grow) as well providing a mathematically traceable and unique solution to the general geolocation

problem. The technique was applied to the 1500-scene SAR data set of the Amazon region collected by JERS-1 over a 62-day period. The resulting error analysis using map-derived ground control points showed that the mosaic was accurately positioning individual scenes to within 400 meters and that correction vectors calculated by the mosaicking method showed systematic offsets induced by the satellite ephemeris. These errors are most likely to have been caused by small timing corrections sent to the satellite on a periodic basis of every ten orbits. In the future we expect that the techniques and analysis presented here will serve as the basis for assembling together future, large-scale SAR data sets in what will provide the scientific community with snap-shot capability of continental sized regions. Indeed, with the accuracies calculated, the compiled radar data obtained from this effort provides an unprecendented synoptic, continental-scale, high-resolution dataset in a digital format suitable for a wide variety of science applications.

VI. Acknowledgments

The work described in this publication was partially carried out by the Jet Propulsion Laboratory, California Institute of Technology, under a contract with the National Aeronautics and Space Administration.

VI. References

Anderson, E., Bai, Z., Bischof, C., Demmel, J.W., Dongarra, J.J., Du Croz, J., Greenbaum, A., Hammarling, S., McKenney, A., and Sorensen, D., "LAPACK: A portable linear algebra library for high-performance computers," Computer Science Dept. Technical Report CS-90-105, University of Tennessee, Knoxville, 1990.

Chapman, B., Alves, M., Shimada, M., Freeman, A., Rosenqvist, A., and Siqueira, P., "Data Quality of the JERS-1 SAR Global Rain Forest Mapping (GRFM) Project," Submitted to International Journal of Remote Sensing, March 1998.

Curlander, J., "Location of Spaceborne SAR Imagery," IEEE Trans. Geosci. Rem. Sens., GE-20(3), 359-364, 1982.

Freeman, A., Chapman, B., and Alves, M., "The JERS-1 Amazon Multi-mission Mapping Study (JAMMS)," Proceedings of the International Society of Geoscience and Remote Sensing, Lincoln, Nebraska, pp 830-833, 1996.

Hensley, S. and Shaffer, S., "Mosaicking of Radar Interferometric DEM Data," in preparation.

Hensley, S. "Mosaicking Principles," UCLA Course Notes, 1996

Hensley, S., Rosen, P., and Zebker, H., "Generation of hight resolution topographic maps of the Galapagos Islands by TOPSAR," Proceedings PIERS Noordwijk, Netherlands, 1994.

Kwok, R., Curlander, J., and Pang, S., "An Automated System of Mosaicking Spaceborne SAR Imagery," Int. J. Rem. Sens., 11(2), 209-223, 1990.

Press, W., Teukolsky, S., Vetterling, W., and Flannery, B., *Numerical Recipes, 2nd Ed.* Cambridge University Press, Cambridge, MA, 1992.

Rosenquist, A., "The Global Rain Forest Mapping Project by JERS-1 SAR," Proc. at XVIII ISPRS Cong. in Vienna, Austria, 1996.